Received: 14 October 2020 | Revised: 21 December 2020 | Accepted: 30 December 2020

DOI: 10.1002/jcp.30273

ORIGINAL RESEARCH ARTICLE

Journal of Cellular Physiology WILEY

Hepatocyte size fractionation allows dissection of human liver zonation

Magnus Ölander[1] | Christine Wegler[1,2] | Inken Flörkemeier[1] | Andrea Treyer[1] | Niklas Handin[1] | Jenny M. Pedersen[1] | Anna Vildhede[1] | André Mateus[1] | Edward L. LeCluyse[3] | Jozef Urdzik[4] | Per Artursson[1,5]

[1]Department of Pharmacy, Uppsala University, Uppsala, Sweden

[2]DMPK, Research and Early Development Cardiovascular Renal and Metabolism, BioPharmaceuticals R&D, AstraZeneca, Gothenburg, Sweden

[3]LifeNet Health, Research Triangle Park, North Carolina, USA

[4]Department of Surgical Sciences, Uppsala University, Uppsala, Sweden

[5]Science for Life Laboratory, Uppsala University, Uppsala, Sweden

Correspondence

Per Artursson, Professor in Drug Delivery, Department of Pharmacy, Uppsala University, Box 580, SE-75123 Uppsala, Sweden.
Email: per.artursson@farmaci.uu.se

Funding information

Swedish Research Council,
Grant/Award Numbers: 01951, 2822, 01586

Abstract

Human hepatocytes show marked differences in cell size, gene expression, and function throughout the liver lobules, an arrangement termed liver zonation. However, it is not clear if these zonal size differences, and the associated phenotypic differences, are retained in isolated human hepatocytes, the "gold standard" for in vitro studies of human liver function. Here, we therefore explored size differences among isolated human hepatocytes and investigated whether separation by size can be used to study liver zonation in vitro. We used counterflow centrifugal elutriation to separate cells into different size fractions and analyzed them with label-free quantitative proteomics, which revealed an enrichment of 151 and 758 proteins (out of 5163) in small and large hepatocytes, respectively. Further analysis showed that protein abundances in different hepatocyte size fractions recapitulated the in vivo expression patterns of previously described zonal markers and biological processes. We also found that the expression of zone-specific cytochrome P450 enzymes correlated with their metabolic activity in the different fractions. In summary, our results show that differences in hepatocyte size matches zonal expression patterns, and that our size fractionation approach can be used to study zone-specific liver functions in vitro.

KEYWORDS

cell separation, cell size, hepatocytes, liver, proteomics

1 | INTRODUCTION

Hepatocytes are the main cell type of the liver, constituting around 80% of its volume (Kmiec, 2001). Structurally, hepatocytes are organized in repeating units of hexagonal lobules, with marked differences in gene expression, differentiation, and function from the periportal region in the lobule periphery to the pericentral region in the middle. This structured heterogeneity, known as liver zonation (Gebhardt & Matz-Soja, 2014), is established by an elaborate interplay between many factors, including concentration gradients of environmental components, like oxygen (Jungermann & Kietzmann, 2000), and various signaling molecules, such as Wnt morphogens (Benhamouche et al., 2006) and glucagon (Cheng et al., 2018). Many liver functions show distinct zonation patterns. For example, periportal hepatocytes are highly involved in gluconeogenesis and urea synthesis, whereas pericentral hepatocytes perform glycolysis and metabolism of xenobiotics (Gebhardt & Matz-Soja, 2014). Zonation is

also apparent in many pathological states of the liver (Ben-Moshe & Itzkovitz, 2019). These include autoimmune hepatitis, which predominantly occurs in the periportal region (Diamantis & Boumpas, 2004), as well as the steatosis and injury associated with fatty liver disease, which first manifest in the pericentral region (Brunt, 2007).

The expression patterns of liver zonation have been extensively characterized on both the messenger RNA (mRNA) and protein levels (Ben-Moshe et al., 2019; Berndt et al., 2020; Brosch et al., 2018; Halpern et al., 2017; MacParland et al., 2018; McEnerney et al., 2017), even though human data is still lacking at the protein level. Some of these studies used computational methods to separate cells from different zones (Halpern et al., 2017; MacParland et al., 2018), while others used laser capture microdissection (Brosch et al., 2018; McEnerney et al., 2017) or fluorescence-activated cell sorting (FACS; Ben-Moshe et al., 2019; Berndt et al., 2020) to perform actual physical separation of cells. While these methods allow highly precise separation and characterization of many cellular subpopulations, they cannot easily be used to obtain cells in the amounts typically required for functional studies in vitro.

Interestingly, liver zonation is accompanied by increasing cell size from the periportal to the pericentral region (Turner et al., 2011). This provides a potentially useful experimental connection between zonal origin and a physical property of the cell. However, while isolated human hepatocytes are widely used in experimental studies of liver biology (Godoy et al., 2013), the properties of human hepatocytes of different sizes in vitro remain largely unexplored. If the connection between zonal origin and cell size is retained after isolation, a technique such as counterflow centrifugal elutriation (Sanderson et al., 1976), which allows the fractionation of massive numbers of cells (up to billions) by size, could be used to facilitate in vitro studies of liver zonation.

In this study, we first confirmed that there is considerable variability in cell size distributions between different batches of isolated human hepatocytes. We then used counterflow centrifugal elutriation to separate human hepatocytes into six size fractions of progressively larger cells. Proteomic analysis revealed that proteins that were enriched in different size fractions largely represented biological processes of known zonal specificity. Finally, we compared the expression and metabolic activity of important cytochrome P450 (CYP) enzymes across the size fractions. We observed strong correlations between expression and metabolic function for CYPs with known zonation in vivo (CYP1A2, CYP2B6, CYP2C19, and CYP3A4), but not for non-zonated CYPs (CYP2D6, CYP2C9, and CYP2C8). Altogether, our results indicate that differences in cell size among isolated human hepatocytes are related to zonal origin, and that elutriation-based size fractionation enables studies of zonated human liver functions in vitro.

2 | MATERIALS AND METHODS

2.1 | Hepatocyte isolation

Liver tissue was obtained from human liver resection surgery at the Department of Surgery, Uppsala University Hospital, Sweden. All donors provided informed consent, in agreement with the approval from the Uppsala Regional Ethical Review Board (Ethical Approval no. 2009/028). Primary hepatocytes were isolated based on a two-step collagenase perfusion technique, as previously described (LeCluyse & Alexandre, 2010). Briefly, the tissue was flushed with HypoThermosol FRS (BioLife Solutions) to remove blood, before transport to the laboratory. Two blood vessels were cannulated and the cut surface was sealed with medical adhesive. The tissue was submerged in warm DPBS and perfused with a calcium-depleted buffer to disrupt cell-cell connections, followed by perfusion with collagenase/protease-containing buffer. After complete digestion, the tissue was placed in warm medium and Glisson's capsule was opened. The tissue was gently shaken and stroked to release hepatocytes into the medium. The cell suspension was filtered and subjected to a series of centrifugation steps, including density centrifugation with Percoll (GE Healthcare), to remove nonparenchymal cells and nonviable hepatocytes.

2.2 | Cryopreservation and thawing

Cryopreservation was performed at 10×10^6 viable hepatocytes per cryovial, followed by storage at −150°C. Vials were thawed in a 37°C water bath for approximately 2 min. Dead cells were removed by density centrifugation.

2.3 | Cell viability and size

Viable cell counts and sizes in cell suspensions were determined with an acridine orange (AO)/propidium iodide (PI) viability assay using a Cellometer Vision CBA image cytometer (Nexcelom Bioscience).

2.4 | Hepatocyte plating and monolayer quality

After thawing, hepatocytes were resuspended in pre-warmed suspension and attachment medium (LeCluyse & Alexandre, 2010) and analyzed with image cytometry as described above. Cells were seeded in 24-well plates coated with Collagen I (Corning) and incubated at 37°C with 5% CO_2. After 3 h in culture, the medium was exchanged for supplemented Hepatocyte Maintenance Medium (complete HMM; Lonza). Monolayer scores, representing monolayer quality (with higher scores indicating higher quality), were assigned after 24 h in culture, as previously described (Ölander et al., 2019). Briefly, the monolayer score is based on qualitative, blinded evaluation of monolayer images, including assessments of cell shape, level of cell stretching, distinctness of cell-cell contacts, presence of dead cells and debris, and the degree of confluence.

2.5 | Cell separation with counterflow centrifugal elutriation

Cryopreserved hepatocytes were thawed and resuspended in ice-cold elutriation buffer (EB), consisting of HBSS with Ca^{2+} and

Mg^{2+}, and 0.2% (w/v) BSA. The cell suspension was filtered through a 70 µm cell strainer and injected into a JE-5.0 elutriation rotor (Beckman Coulter) set up with the small elutriation chamber, in an Avanti J-20 XPI centrifuge (Beckman Coulter) at a speed of 2500 rpm and an EB flow rate of 32 ml/min. The centrifuge and buffer were kept at 4°C. Centrifugation speeds and flow rates were gradually adjusted for sequential elutriation of six different size fractions (Table S5). A volume of 100 ml was collected for each fraction and kept on ice. The fractions were centrifuged at 75 *g* for 5 min at 4°C, and supernatants were removed. Cell pellets were resuspended in medium as necessary for the intended experiment, or stored at −80°C pending proteomic analysis.

2.6 | Proteomic analysis

Samples were prepared for proteomic analysis using multi-enzyme digestion filter-aided sample preparation (MED-FASP), with Lys-C and trypsin (Wiśniewski & Mann, 2012). Total protein and peptide amounts were determined based on tryptophan fluorescence (Wiśniewski & Gaugaz, 2015). Proteomic analysis was performed with a Q Exactive HF mass spectrometer (Thermo Fisher Scientific). MS data was processed with MaxQuant (Cox & Mann, 2008). Protein copy numbers were calculated with the Proteomic Ruler approach (Wiśniewski et al., 2014). The mass spectrometry proteomics data have been deposited to the ProteomeXchange Consortium via the PRIDE partner repository (Vizcaino et al., 2016) with the data set identifier PXD013142.

2.7 | CYP activity

Elutriated hepatocyte fractions were resuspended in complete HMM and incubated with probe drugs to monitor the activities of CYP3A4, CYP2D6, CYP2B6, CYP2C8, CYP2C9, CYP2C19, and CYP1A2. Drug clearance was analyzed by a substrate depletion method (Obach, 1999), using UPLC-MS/MS detection.

2.8 | Statistical analysis

Frequency distributions and statistical tests were performed using GraphPad Prism, version 7.03. Pathway analysis was performed by functional annotation clustering in version 6.8 of the DAVID database (Huang et al., 2008), including GOBP, GOCC, and KEGG terms, using the default settings. Annotation clusters were considered significant at enrichment scores above 1.3 (corresponding to *p*-values < .05). Transcription factor analysis was performed with the FunRich software, version 3.1.3 (Pathan et al., 2015).

Extended method descriptions are available in the Supporting Information.

TABLE 1 Donor characteristics of the human hepatocyte batches included in this study

Characteristic[a]	All batches, *n* = 54
Age, years, median (IQR)	68 (57–73)
Gender	
Male	34 (63%)
Female	20 (37%)
BMI, median (IQR)	24.6 (22.8–28.7)
Diagnosis	
Colorectal cancer	43 (80%)
Gastrointestinal stromal tumor	2 (3.7%)
Malignant melanoma	2 (3.7%)
Adenoma	1 (1.9%)
Small intestine cancer	2 (3.7%)
Hepatocellular carcinoma	2 (3.7%)
Bile duct cancer	1 (1.9%)
Breast cancer	1 (1.9%)
Cytostatic treatment	41 (76%)

[a]Data for individual donors can be found in Table S1.

3 | RESULTS

3.1 | Size distributions in unfractionated human hepatocyte batches

Human hepatocytes show marked size differences along the periportal-pericentral axis (Turner et al., 2011). To investigate if these differences are retained after isolation, we used all available data from our collection of isolated human hepatocytes (Tables 1 and S1), obtained with a two-step collagenase perfusion technique (LeCluyse & Alexandre, 2010), to evaluate the cell size variability between different hepatocyte batches (54 cryopreserved batches in total). We found that, on average, freshly isolated (*n* = 48, including eight batches that were not cryopreserved) and cryopreserved batches (*n* = 54) had very similar size distributions, indicating that size distributions are not affected by cryopreservation (Figures 1a and S1). We therefore focused solely on cryopreserved hepatocytes, as these are more commonly used in practice. Median cell size (diameter) in the 54 cryopreserved batches (Figure S2) was 18.4 µm and most cells (88%) had diameters between 12 and 26 µm. Interestingly, size distributions of cryopreserved hepatocytes showed high inter-batch variability. Distribution maxima ranged from 14 to 22 µm, and the distributions had different shapes (Figure 1b). Using our recently described scoring metric (termed monolayer score) for morphological evaluation of hepatocyte quality after cryopreservation (Ölander et al., 2019), we found that overall inter-batch size variability was generally unrelated to differences in batch quality (Figure S3). Importantly, size distributions in individual hepatocyte batches were (almost) identical at different thawing occasions (i.e., using cells from different cryovials), demonstrating the reproducibility of our cell size

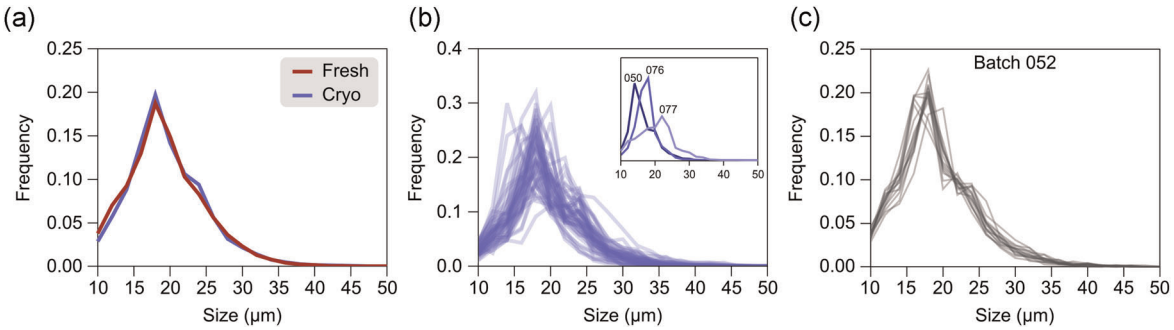

FIGURE 1 Size characteristics of isolated human hepatocytes. (a) Average cell size distributions of freshly isolated and cryopreserved hepatocyte batches, using all our available size data ($n = 48$ and $n = 54$ for fresh and cryopreserved batches, respectively). (b) Size distributions of cryopreserved hepatocyte batches, highlighting the considerable variability between batches. Inset are three examples of highly different batches (050, 076, and 077). (c) Representative example of a cryopreserved hepatocyte batch (052) that was thawed and analyzed multiple times (i.e., with cells from different cryovials), showing that size distributions are highly reproducible

measurements (Figures 1c and S2). Together, our results show that cells of different sizes are retained after isolation of human hepatocytes, and that hepatocyte batches differ in cell size composition.

3.2 | Size separation of human hepatocytes

To further probe hepatocyte size characteristics, we used counterflow centrifugal elutriation to separate 10 cryopreserved hepatocyte batches, representing the full range of monolayer scores, into six size fractions (F1–F6; see Table S1 for batch use). Median cell size ranged from 15.9 μm (IQR: 14.6–17.0 μm) in F1 to 20.9 μm (IQR: 19.0–23.2 μm) in F6 (Figure 2a). The percentage of total cells belonging to different fractions was highly variable between batches (Figure 2b), in line with the inter-batch variability in size distributions. On average, F4 contained the most cells (22% of total), but all fractions generally contained over 10% of total cells (Figure 2c). Overall, these results show that our elutriation protocol can yield hepatocyte fractions of progressively larger cell size with experimentally useful numbers of cells in all fractions.

3.3 | Proteomic analysis of hepatocyte size fractions

We next performed global proteomic analysis of different size fractions from three batches (029, 051, and 085; see Table S1), together with corresponding unfractionated controls. The batches we included thus originated from different donors (and, consequently, had different size distributions), to avoid generating data that would only be meaningful for a specific donor. In total, we identified 5163 proteins, with only a few proteins unique to each fraction (Figures 3a and S4). The full data set can be found in Table S2. However, all fractions contained proteins that differed from expression levels in the unfractionated controls (Figure 3b). To rule out contamination by nonparenchymal cells (NPCs), we examined the expression of reliably quantified markers (i.e., detected by at least three unique peptides) for the major NPC types, that is, liver sinusoidal endothelial cells (LSEC), Kupffer cells (KC), and hepatic stellate cells (HSC; Ölander et al., 2020). We investigated markers that were previously found at low but detectable levels in unfractionated hepatocyte batches (Vildhede et al., 2015). NPCs are generally smaller than hepatocytes (Kegel et al., 2016), and could potentially contaminate our early

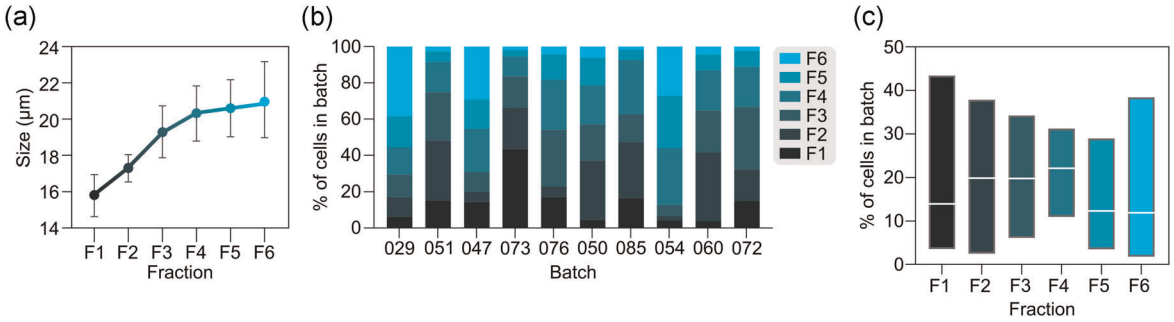

FIGURE 2 Size separation of cryopreserved human hepatocytes using counterflow centrifugal elutriation. (a) Cell size in the different size fractions ($n = 10$ batches). Dots show medians and error bars denote interquartile ranges. (b) Percentage of total cells belonging to different size fractions in 10 hepatocyte batches, sorted by monolayer score. (c) Range (min to max) of batch content of different size fractions. White lines show means

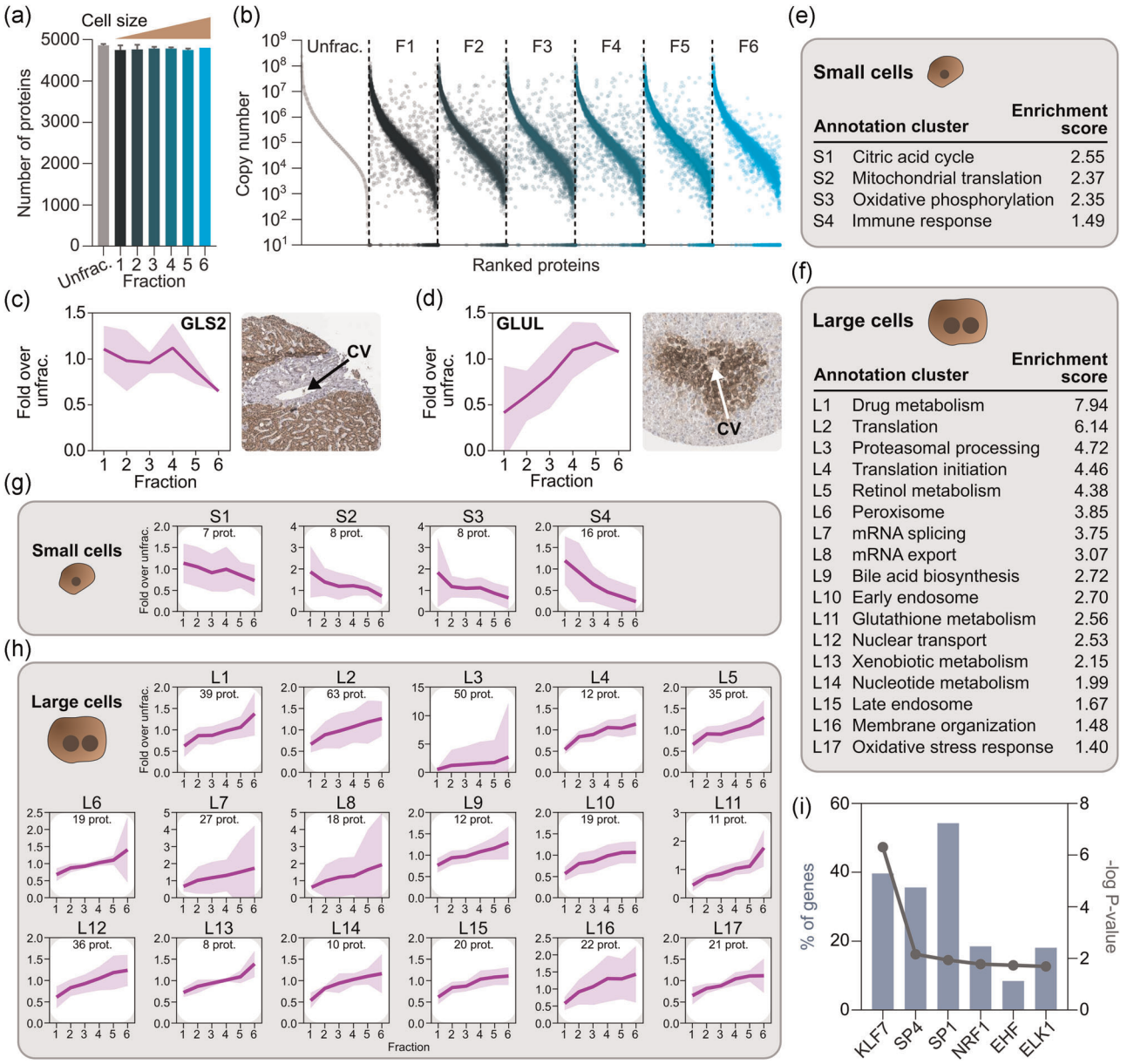

FIGURE 3 Global proteomic analysis of different size fractions of cryopreserved human hepatocytes. (a) Number of proteins detected in different size fractions from the three batches (029, 051, and 085) that were analyzed with label-free quantitative proteomic analysis. (b) Identified proteins ranked by abundance in the unfractionated controls. (c) and (d) Protein abundance of (c) the periportal marker GLS2 and (d) the pericentral marker GLUL, shown as fold over unfractionated controls. Shaded areas denote standard deviations. Histological images of GLS2 and GLUL expression in human liver (from the HPA) show similar patterns. Central veins (CV) are marked with arrows. (e) and (f) Enriched biological functions in (e) small and (f) large hepatocytes. Enrichment scores denote the statistical significance of the functional annotation clusters from the pathway analysis (see Section 2). (g) and (h) Average expression profiles of proteins in individual enrichment clusters from (g) small cells and (h) large cells. (i) Transcription factors predicted to be involved in regulating the expression of enriched proteins in large hepatocytes

fractions containing small hepatocytes. Encouragingly, virtually no NPC markers were detected, except for very low levels of one LSEC marker (STAB1) in two samples (Figure S5). Blood cells constitute another potential contaminant, and we therefore investigated the expression of common markers for erythrocytes, T cells, and B cells. However, none of the blood cell markers were detected (Figure S5). These results indicate that our elutriation approach generates hepatocyte fractions essentially free from NPCs and blood cells.

We then investigated the size-dependent expression of two well-known markers of liver zonation, glutaminase 2 (GLS2) and glutamine synthetase (GLUL), which are predominantly expressed in the periportal and pericentral regions, respectively, and play important roles in ammonia detoxification (Ghafoory et al., 2013). GLS2 and GLUL showed distinct enrichment patterns that matched histological images of human liver tissue from the Human Protein Atlas (Uhlén et al., 2015; HPA; Figure 3c,d). Thus, GLS2 expression was relatively even in F1–F4 and

decreased in the large cells from F5–F6, whereas GLUL expression steadily increased from small to large cells. Furthermore, we compared our data with a transcriptomic study of laser microdissected zones from human liver tissue, selecting genes with predominant expression in periportal and pericentral hepatocytes (McEnerney et al., 2017). We observed similar trends in the average expression profiles of these genes in our size fractions. In large cells, expression of pericentral genes was markedly enriched, and periportal genes depleted (Figure S6). Periportal genes were also expressed at lower levels in the first fraction, which may indicate a difference between mRNA and protein levels in very small hepatocytes. Generally, the expression patterns we observed provide additional support for the connection between cell size and zonal origin.

To identify more proteins with sequential enrichment across fractions, we correlated protein abundance with fraction numbers (1–6). We considered proteins with a Pearson's correlation coefficient below −.8 or above .8 to be enriched in small and large hepatocytes, respectively. Using these criteria, we found that 151 proteins were enriched in small cells, while 758 proteins showed enrichment in large cells, corresponding to enriched expression in periportal and pericentral hepatocytes, respectively (Table S3). The higher number of proteins with enrichment in large cells is in agreement with studies of zonal RNA and protein levels in murine liver, where larger proportions of non-randomly zonated genes were pericentrally enriched (Ben-Moshe et al., 2019; Halpern et al., 2017).

Pathway analysis showed that clusters of enriched proteins represented many biological processes with known zonal specificity. Small hepatocytes showed significant enrichment of proteins involved in the immune response and oxidative energy metabolism (Figure 3e and Table S4). The latter is consistent with the high oxygen concentration in the periportal region (Jungermann & Kietzmann, 2000). Energy metabolism proteins included all three subunits of isocitrate dehydrogenase, a key enzyme of the citric acid cycle, and several subunits of protein complexes in the mitochondrial respiratory chain. Large hepatocytes, on the other hand, showed significant enrichment of many pericentral processes (Figure 3f and Table S4), such as drug metabolism, peroxisomal processes, bile acid biosynthesis, glutathione metabolism, and oxidative stress responses (Gebhardt & Matz-Soja, 2014). The drug metabolism cluster contained members of several important families of metabolic enzymes, including nine CYPs, five glutathione S-transferases (GSTs), and seven UDP-glucuronosyltransferases (UGTs). Interestingly, although not part of the drug metabolism cluster in the enrichment analysis, the uptake transporter SLCO1B3 was also enriched in large cells. However, most clinically relevant drug transporters (Zamek-Gliszczynski et al., 2018) were not notably zonated (Figure S7). Closer inspection of expression patterns in individual enrichment clusters confirmed the findings of the pathway analysis (Figure 3g,h).

We then performed predictions of which transcription factors (TFs) could be involved in regulating the expression of enriched proteins in small and large hepatocytes. No clear results were found for proteins enriched in small cells, but six TFs (KLF7, SP4, SP1, NRF1, EHF, and ELK1) were predicted to be involved in regulating a large proportion of proteins enriched in large cells (Figure 3i). In relation to the pathway analysis, it is interesting to note the association of SP1 with the hepatocyte response to hepatotoxins (Reymann & Borlak, 2006) and the importance of NRF1 in oxidative stress protection in the liver (Xu et al., 2005). These, as well as other associated TFs, merit additional study for further elucidation of the molecular determinants of liver zonation.

3.4 | Zonated functionality in hepatocyte size fractions

Finally, we assessed whether the differences in protein expression across fractions were reflected by differences in hepatocyte functionality. To this end, we analyzed the metabolic activity of the seven most important CYP enzymes in hepatic drug metabolism, that is, CYP3A4, CYP2D6, CYP2C9, CYP1A2, CYP2B6, CYP2C19, and CYP2C8 (Zanger & Schwab, 2013). Experiments were performed with cell suspensions immediately after size separation (starting with approximately 50 million cryopreserved cells per batch), at a concentration of 1×10^6 cells/ml. Four of the enzymes (CYP1A2, CYP2B6, CYP2C19, and CYP3A4) showed strong correlations between expression and activity across fractions ($r_s = .94$, $p = .017$; Figure 4a). Histological images of human liver from the HPA matched these patterns, showing predominant expression in the pericentral region (Figure 4b). The results on CYP expression and activity are further supported by previous studies on the zonal expression patterns of these enzymes in human liver (Lindros, 1997; McEnerney et al., 2017). These results demonstrate that zonal differences in hepatocyte function are carried over to isolated hepatocyte batches in vitro.

4 | DISCUSSION

Here, we show that cell size in isolated human hepatocytes is connected with zonal origin. This can be utilized to separate hepatocytes into zone-specific fractions with retained protein expression patterns and function. Accordingly, the size fractionation approach we describe constitutes a convenient tool to study liver zonation using isolated human hepatocytes.

The transcriptomic and proteomic characteristics of mammalian liver zonation have recently been comprehensively investigated (Ben-Moshe et al., 2019; Brosch et al., 2018; Halpern et al., 2017; MacParland et al., 2018; McEnerney et al., 2017), but human proteomic data has not previously been described. The proteomic data from different size fractions of human hepatocytes that we describe here constitutes an effort to address this, and the biological functions enriched in our data were largely in agreement with previous studies. Specifically, the relevance of our proteomic results in a liver zonation context is supported by comparisons with a previous transcriptomic analysis of laser microdissected zones from human liver tissue (McEnerney et al., 2017) and with histological images of zonal expression patterns from the Human Protein Atlas (Uhlén et al., 2015). This indicates that size separation is a useful tool for studying liver zonation. An interesting aspect of small hepatocytes, revealed by our proteomic data, was the enrichment of some immune response proteins, particularly related to antigen presentation.

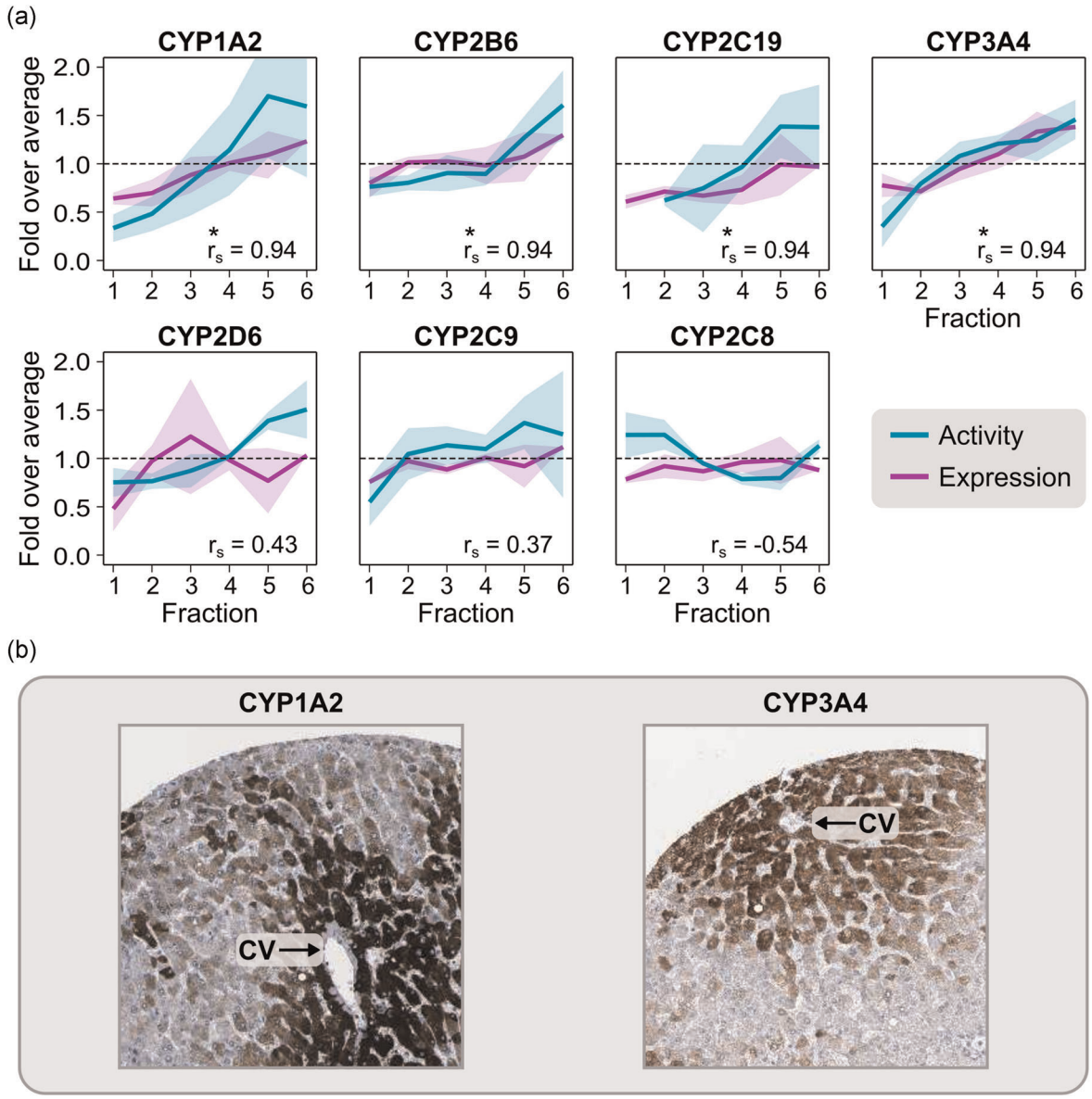

FIGURE 4 Analysis of the connection between protein abundance and zonated functionality across hepatocyte size fractions. (a) Expression and metabolic activity of important CYP enzymes, used to represent hepatocyte function. CYP activity and expression is shown as fold over the average of all fractions ($n = 2$ batches). Experiments were performed at a concentration of 1×10^6 cells/ml. Shaded areas denote standard deviations. (b) Similar zonation patterns can be observed in histological images of human liver from the HPA, shown here for CYP1A2 and CYP3A4. Central veins (CV) are marked with arrows. r_s, Spearman's correlation coefficient

Hepatocytes are known to express major histocompatibility complex (MHC) molecules involved in antigen presentation (Chen et al., 2005), and these findings may point to a periportal preference for this function. This could be linked to the fact that periportal hepatocytes are the first to encounter and process gut-derived antigens (Robinson et al., 2016).

The proteomic results were supported by our observations (in batches that were also used for proteomics) on the size-dependent metabolic activity of four CYP enzymes with known zonated expression patterns (CYP1A2, CYP2B6, CYP2C19, and CYP3A4), further indicating that there is a connection between cell size and zonal origin. Size fractionation should thus also be useful for exploring other zonated liver functions. For instance, the prominent zonation of metabolic enzymes is thought to underlie the zone-specific hepatotoxicity of some xenobiotics, such as carbon tetrachloride and acetaminophen (Lindros, 1997). Acetaminophen is converted into a toxic metabolite by the pericentral CYP enzymes CYP2E1, CYP1A2, and CYP3A4 (Kang et al., 2018), which we show are enriched in the large hepatocytes that populate this region. Interestingly, zonal differences in CYP3A4 expression have, together with estimations of sinusoidal blood flow, been incorporated in pharmacokinetic models of midazolam clearance (a CYP3A4 substrate), providing a detailed picture of decreasing concentrations along a sinusoid, with the major metabolic contribution coming from pericentral hepatocytes (Schwen et al., 2015). The data we provide here could be used to refine such models for any enzyme of interest.

We also observed enrichment of the UGT family of Phase II metabolic enzymes in large cells, in line with previous studies showing predominantly pericentral expression of UGT enzymes (Lindros, 1997; Mouelhi & Kauffman, 1986). On the other hand, zonation does not seem to be as prominent for hepatic drug transporters (Li et al., 2009). Indeed, we found that most clinically important solute carrier (SLC) and ATP-binding cassette (ABC) transporters (Zamek-Gliszczynski et al., 2018) did not show size-dependent enrichment of expression, in line with a study of transporter expression in murine liver (Tachikawa et al., 2018). Nevertheless, the uptake transporter SLCO1B3 showed clear enrichment in large cells. Supporting this, SLCO1B3 was the sixth most strongly enriched protein in the pericentral region in a study of laser microdissected human liver tissue (McEnerney et al., 2017).

We conclude that our approach can be used to facilitate functional studies of human liver zonation in vitro, as cell separation with counterflow centrifugal elutriation can be readily performed with cryopreserved hepatocytes. Other methods for separation of periportal and pericentral hepatocytes, such as digitonin-collagenase perfusion (Quistorff, 1985), typically require fresh liver tissue. Fresh human liver tissue for hepatocyte isolation is not routinely available for most researchers, and the possibility of using cryopreserved cells provides experimental flexibility. Further optimization of the elutriation procedure may give even more clear separation of zone-specific functions, but our analyses demonstrate the usefulness of the present protocol. In fact, size fractionation by elutriation has previously been used in small-scale studies of zonation in rodent hepatocytes (Gumucio et al., 1986). However, due to species differences in liver structure and function, the results from such studies may not be directly translatable to humans (Akiyoshi et al., 1998; Martignoni et al., 2006), highlighting the need for the type of human-adapted protocol we describe here.

We found that all size fractions generally contained over 10% of total cells, meaning that a crude rule of thumb for experimentation would be to start with more than 20 million cells to obtain at least 2 million cells per fraction for functional studies, but we recommend using around twice the required number (if possible) to account for batch-to-batch variability in yields. While the elutriation technique cannot provide the detailed subpopulation resolution of carefully designed FACS-based approaches (Ben-Moshe et al., 2019), an advantage is that it works well with much larger cell quantities: hundreds of millions, or even billions, of cells can be rapidly processed at the same time without adjustments to the protocol. This means that very large numbers of cells can be obtained for each fraction if required for the intended experiment. Another interesting aspect of elutriation, worthy of further exploration, is that it can be used to isolate different types of NPCs from digested liver tissue (Knook & Sleyster, 1976). NPCs differ in size and are all, in general, considerably smaller than hepatocytes (Kegel et al., 2016). This implies that an elutriation protocol could be designed for the sequential isolation of NPCs and periportal, midlobular, and pericentral hepatocytes in a single run.

In summary, our results suggest that hepatocyte size is associated with zonal origin, and that zonal differences in proteome composition and hepatocyte function are carried over to isolated batches in vitro. This was reinforced by the strong correlations we observed between protein expression and function of important zonated CYP enzymes across different hepatocyte size fractions. Our fractionation approach thus enables experimental applications beyond the possibilities of whole-batch experiments, and benefits the exploration of zonal differences in human liver function in health and disease.

ACKNOWLEDGMENTS

We thank Elin Khan, Maria Mastej, Maria Backlund, and Patrik Lundquist at the Department of Pharmacy, Uppsala University, for technical assistance with hepatocyte isolation. This study was supported by the Swedish Research Council, grants no. 2822, 01951, and 01586.

CONFLICT OF INTERESTS

The authors declare that there are no conflicts of interests.

AUTHOR CONTRIBUTIONS

Magnus Ölander, Christine Wegler, Andrea Treyer, André Mateus, and Per Artursson conceived and designed the study. Jozef Urdzik provided human liver tissue. Magnus Ölander, Christine Wegler, Andrea Treyer, Niklas Handin, Jenny M. Pedersen, Anna Vildhede, André Mateus, and Edward L. LeCluyse performed hepatocyte isolation. Magnus Ölander, Christine Wegler, Andrea Treyer, and Inken Flörkemeier performed experiments. Magnus Ölander, Christine Wegler, Andrea Treyer, Inken Flörkemeier, André Mateus, Jozef Urdzik, and Per Artursson analyzed and interpreted data. Magnus Ölander and Per Artursson wrote the manuscript with input from all authors.

DATA AVAILABILITY STATEMENT

The proteomics data that support the findings of this study are openly available through the ProteomeXchange Consortium via the PRIDE partner repository with the data set identifier PXD013142.

ORCID

Magnus Ölander https://orcid.org/0000-0002-4502-8184
Per Artursson https://orcid.org/0000-0002-3708-7395

REFERENCES

Akiyoshi, H., Gonda, T., & Terada, T. (1998). A comparative histochemical and immunohistochemical study of aminergic, cholinergic and peptidergic innervation in rat, hamster, guinea pig, dog and human livers. *Liver*, *18*(5), 352–359.

Benhamouche, S., Decaens, T., Godard, C., Chambrey, R., Rickman, D. S., Moinard, C., & Colnot, S. (2006). Apc tumor suppressor gene is the "zonation-keeper" of mouse liver. *Developmental Cell*, *10*(6), 759–770.

Ben-Moshe, S., & Itzkovitz, S. (2019). Spatial heterogeneity in the mammalian liver. *Nature Reviews Gastroenterology & Hepatology*, *16*(7), 395–410.

Ben-Moshe, S., Shapira, Y., Moor, A. E., Manco, R., Veg, T., Bahar Halpern, K., & Itzkovitz, S. (2019). Spatial sorting enables comprehensive characterization of liver zonation. *Nature Metabolism*, *1*(9), 899–911.

Berndt, N., Kolbe, E., Gajowski, R., Eckstein, J., Ott, F., Meierhofer, D., & Matz-Soja, M. (2020). Functional consequences of metabolic

zonation in murine livers: New insights for an old story. *Hepatology*, hep.31274

Brosch, M., Kattler, K., Herrmann, A., von Schönfels, W., Nordström, K., Seehofer, D., & Hampe, J. (2018). Epigenomic map of human liver reveals principles of zonated morphogenic and metabolic control. *Nature Communications*, *9*(1), 4150.

Brunt, E. M. (2007). Pathology of fatty liver disease. *Modern Pathology*, *20*(1), S40–S48.

Chen, M., Tabaczewski, P., Truscott, S. M., Van Kaer, L., & Stroynowski, I. (2005). Hepatocytes express abundant surface class I MHC and efficiently use transporter associated with antigen processing, tapasin, and low molecular weight polypeptide proteasome subunit components of antigen processing and presentation pathway. *Journal of Immunology*, *175*(2), 1047–1055.

Cheng, X., Kim, S. Y., Okamoto, H., Xin, Y., Yancopoulos, G. D., Murphy, A. J., & Gromada, J. (2018). Glucagon contributes to liver zonation. *Proceedings of the National Academy of Sciences of the United States of America*, *115*(17), E4111–E4119.

Cox, J., & Mann, M. (2008). MaxQuant enables high peptide identification rates, individualized ppb-range mass accuracies and proteome-wide protein quantification. *Nature Biotechnology*, *26*(12), 1367–1372.

Diamantis, I., & Boumpas, D. T. (2004). Autoimmune hepatitis: Evolving concepts. *Autoimmunity Reviews*, *3*(3), 207–214.

Gebhardt, R., & Matz-Soja, M. (2014). Liver zonation: Novel aspects of its regulation and its impact on homeostasis. *World Journal of Gastroenterology*, *20*(26), 8491–8504.

Ghafoory, S., Breitkopf-Heinlein, K., Li, Q., Scholl, C., Dooley, S., & Wölfl, S. (2013). Zonation of nitrogen and glucose metabolism gene expression upon acute liver damage in mouse. *PLoS One*, *8*(10), e78262.

Godoy, P., Hewitt, N. J., Albrecht, U., Andersen, M. E., Ansari, N., Bhattacharya, S., & Boettger, J. (2013). Recent advances in 2D and 3D in vitro systems using primary hepatocytes, alternative hepatocyte sources and non-parenchymal liver cells and their use in investigating mechanisms of hepatotoxicity, cell signaling and ADME. *Archives of Toxicology*, *87*(8), 1315–1530.

Gumucio, J. J., May, M., Dvorak, C., Chianale, J., & Massey, V. (1986). The isolation of functionally heterogeneous hepatocytes of the proximal and distal half of the liver acinus in the rat. *Hepatology*, *6*(5), 932–944.

Halpern, K. B., Shenhav, R., Matcovitch-Natan, O., Tóth, B., Lemze, D., Golan, M., & Itzkovitz, S. (2017). Single-cell spatial reconstruction reveals global division of labour in the mammalian liver. *Nature*, *542*(7641), 352–356.

Huang, D. W., Sherman, B. T., & Lempicki, R. A. (2008). Systematic and integrative analysis of large gene lists using DAVID bioinformatics resources. *Nature Protocols*, *4*(1), 44–57.

Jungermann, K., & Kietzmann, T. (2000). Oxygen: Modulator of metabolic zonation and disease of the liver. *Hepatology*, *31*(2), 255–260.

Kang, Y. B. A., Eo, J., Mert, S., Yarmush, M. L., & Usta, O. B. (2018). Metabolic patterning on a chip: Towards in vitro liver zonation of primary rat and human hepatocytes. *Scientific Reports*, *8*(1), 8951.

Kegel, V., Deharde, D., Pfeiffer, E., Zeilinger, K., Seehofer, D., & Damm, G. (2016). Protocol for isolation of primary human hepatocytes and corresponding major populations of non-parenchymal liver cells. *Journal of Visualized Experiments*, *109*, e53069.

Kmiec, Z. (2001). Cooperation of liver cells in health and disease. *Advances in Anatomy, Embryology and Cell Biology*, *161*, 1–151.

Knook, D. L., & Sleyster, E. C. (1976). Separation of Kupffer and endothelial cells of the rat liver by centrifugal elutriation. *Experimental Cell Research*, *99*(2), 444–449.

LeCluyse, E. L., & Alexandre, E. (2010). Isolation and culture of primary hepatocytes from resected human liver tissue. In P. Maurel, (Ed.), *Hepatocytes: Methods in molecular biology (methods and protocols)* (Vol. 640, pp. 57–82). Humana Press.

Li, P., Wang, G.-J., Robertson, T. A., & Roberts, M. S. (2009). Liver transporters in hepatic drug disposition: An update. *Current Drug Metabolism*, *10*(5), 482–498.

Lindros, K. O. (1997). Zonation of cytochrome P450 expression, drug metabolism and toxicity in liver. *General Pharmacology*, *28*(2), 191–196.

MacParland, S. A., Liu, J. C., Ma, X.-Z., Innes, B. T., Bartczak, A. M., Gage, B. K., & Linares, I. (2018). Single cell RNA sequencing of human liver reveals distinct intrahepatic macrophage populations. *Nature Communications*, *9*(1), 4383.

Martignoni, M., Groothuis, G. M. M., & de Kanter, R. (2006). Species differences between mouse, rat, dog, monkey and human CYP-mediated drug metabolism, inhibition and induction. *Expert Opinion on Drug Metabolism & Toxicology*, *2*(6), 875–894.

McEnerney, L., Duncan, K., Bang, B.-R., Elmasry, S., Li, M., Miki, T., & Saito, T. (2017). Dual modulation of human hepatic zonation via canonical and non-canonical Wnt pathways. *Experimental & Molecular Medicine*, *49*(12), e413.

Mouelhi, M. E., & Kauffman, F. C. (1986). Sublobular distribution of transferases and hydrolases associated with glucuronide, sulfate and glutathione conjugation in human liver. *Hepatology*, *6*(3), 450–456.

Obach, R. S. (1999). Prediction of human clearance of twenty-nine drugs from hepatic microsomal intrinsic clearance data: An examination of in vitro half-life approach and nonspecific binding to microsomes. *Drug Metabolism and Disposition: The Biological Fate of Chemicals*. *27*(11), 1350–1359.

Ölander, M., Wiśniewski, J. R., & Artursson, P. (2020). Cell-type-resolved proteomic analysis of the human liver. *Liver International*, *40*(7), 1770–1780.

Ölander, M., Wiśniewski, J. R., Flörkemeier, I., Handin, N., Urdzik, J., & Artursson, P. (2019). A simple approach for restoration of differentiation and function in cryopreserved human hepatocytes. *Archives of Toxicology*, *93*(3), 819–829.

Pathan, M., Keerthikumar, S., Ang, C. S., Gangoda, L., Quek, C. Y., Williamson, N. A., & Mathivanan, S. (2015). FunRich: An open access standalone functional enrichment and interaction network analysis tool. *Proteomics*, *15*(15), 2597–2601.

Quistorff, B. (1985). Gluconeogenesis in periportal and perivenous hepatocytes of rat liver, isolated by a new high-yield digitonin/collagenase perfusion technique. *Biochemical Journal*, *229*(1), 221–226.

Reymann, S., & Borlak, J. (2006). Transcriptome profiling of human hepatocytes treated with Aroclor 1254 reveals transcription factor regulatory networks and clusters of regulated genes. *BMC Genomics*, *7*, 217.

Robinson, M. W., Harmon, C., & O'Farrelly, C. (2016). Liver immunology and its role in inflammation and homeostasis. *Cellular & Molecular Immunology*, *13*(3), 267–276.

Sanderson, R. J., Bird, K. E., Palmer, N. F., & Brenman, J. (1976). Design principles for a counterflow centrifugation cell separation chamber. *Analytical Biochemistry*, *71*(2), 615–622.

Schwen, L. O., Schenk, A., Kreutz, C., Timmer, J., Bartolome Rodriguez, M. M., Kuepfer, L., & Preusser, T. (2015). Representative sinusoids for hepatic four-scale pharmacokinetics simulations. *PLoS One*, *10*(7), e0133653.

Tachikawa, M., Sumiyoshiya, Y., Saigusa, D., Sasaki, K., Watanabe, M., Uchida, Y., & Terasaki, T. (2018). Liver zonation index of drug transporter and metabolizing enzyme protein expressions in mouse liver acinus. *Drug Metabolism and Disposition: The Biological Fate of Chemicals*. *46*(5), 610–618.

Turner, R., Lozoya, O., Wang, Y., Cardinale, V., Gaudio, E., Alpini, G., & Reid, L. M. (2011). Human hepatic stem cell and maturational liver lineage biology. *Hepatology*, *53*(3), 1035–1045.

Uhlén, M., Fagerberg, L., Hallstrom, B. M., Lindskog, C., Oksvold, P., Mardinoglu, A., & Ponten, F. (2015). Tissue-based map of the human proteome. *Science*, *347*(6220), 1260419.

Vildhede, A., Wiśniewski, J. R., Norén, A., Karlgren, M., Artursson, & P. (2015). Comparative proteomic analysis of human liver tissue and isolated hepatocytes with a focus on proteins determining drug exposure. *Journal of Proteome Research*, *14*(8), 3305–3314.

Vizcaino, J. A., Csordas, A., del-Toro, N., Dianes, J. A., Griss, J., Lavidas, I., & Hermjakob, H. (2016). 2016 update of the PRIDE database and its related tools. *Nucleic Acids Research*, *44*(D1), D447–D456.

Wiśniewski, J. R., & Gaugaz, F. Z. (2015). Fast and sensitive total protein and peptide assays for proteomic analysis. *Analytical Chemistry*, *87*(8), 4110–4116.

Wiśniewski, J. R., Hein, M. Y., Cox, J., Mann, & M. (2014). A 'proteomic ruler' for protein copy number and concentration estimation without spike-in standards. *Molecular & Cellular Proteomics*, *13*(12), 3497–3506.

Wiśniewski, J. R., & Mann, M. (2012). Consecutive proteolytic digestion in an enzyme reactor increases depth of proteomic and phosphoproteomic analysis. *Analytical Chemistry*, *84*(6), 2631–2637.

Xu, Z., Chen, L., Leung, L., Yen, T. S., Lee, C., & Chan, J. Y. (2005). Liver-specific inactivation of the Nrf1 gene in adult mouse leads to nonalcoholic steatohepatitis and hepatic neoplasia. *Proceedings of the National Academy of Sciences of the United States of America*, *102*(11), 4120–4125.

Zamek-Gliszczynski, M. J., Taub, M. E., Chothe, P. P., Chu, X., Giacomini, K. M., Kim, R. B., & Zhang, Y. (2018). Transporters in drug development: 2018 ITC recommendations for transporters of emerging clinical importance. *Clinical Pharmacology and Therapeutics*, *104*(5), 890–899.

Zanger, U. M., & Schwab, M. (2013). Cytochrome P450 enzymes in drug metabolism: Regulation of gene expression, enzyme activities, and impact of genetic variation. *Pharmacology and Therapeutics*, *138*(1), 103–141.

SUPPORTING INFORMATION

Additional Supporting Information may be found online in the supporting information tab for this article.

How to cite this article: Ölander M, Wegler C, Flörkemeier I, et al. Hepatocyte size fractionation allows dissection of human liver zonation. *J Cell Physiol*. 2021;236:5885–5894. https://doi.org/10.1002/jcp.30273